



**HAL**  
open science

**Two novel macrocyclic organotin (IV) carboxylates  
based on bipyrazoledicarboxylic acid derivatives:  
Syntheses, crystal structures and antifungal activities**

Mohammed Dahmani, Tarik Harit, Abdelkader Et-Touhami, Abderrahmane  
Yahyi, Driss Eddike, Monique Tillard, Redouane Benabbes

► **To cite this version:**

Mohammed Dahmani, Tarik Harit, Abdelkader Et-Touhami, Abderrahmane Yahyi, Driss Eddike, et al.. Two novel macrocyclic organotin (IV) carboxylates based on bipyrazoledicarboxylic acid derivatives: Syntheses, crystal structures and antifungal activities. *Journal of Organometallic Chemistry*, 2021, 948, pp.121913. 10.1016/j.jorganchem.2021.121913 . hal-03288001

**HAL Id: hal-03288001**

**<https://hal.umontpellier.fr/hal-03288001v1>**

Submitted on 29 Sep 2021

**HAL** is a multi-disciplinary open access archive for the deposit and dissemination of scientific research documents, whether they are published or not. The documents may come from teaching and research institutions in France or abroad, or from public or private research centers.

L'archive ouverte pluridisciplinaire **HAL**, est destinée au dépôt et à la diffusion de documents scientifiques de niveau recherche, publiés ou non, émanant des établissements d'enseignement et de recherche français ou étrangers, des laboratoires publics ou privés.

# **Two novel macrocyclic organotin (IV) carboxylates based on bipyrazoledicarboxylic acid derivatives: syntheses, crystal structures and antifungal activities.**

Mohammed Dahmani<sup>a</sup>, Tarik Harit<sup>a</sup>, Abdelkader Et-touhami<sup>a,\*</sup>, Abderrahmane Yahyi<sup>a</sup>,  
Driss Eddike<sup>b</sup>, Monique Tillard<sup>c</sup>, Redouane Benabbes<sup>d</sup>.

<sup>a</sup>*Laboratory of Applied Chemistry and Environment –ECOMP, Faculty of Sciences, Mohammed First University Bd Mohamed VI, BP: 717, Oujda 60000, Morocco.*

<sup>b</sup>*Laboratory of Applied Chemistry and Environment-CSM, Faculty of Sciences, Mohamed First University, Bd Mohamed VI, BP 717, Oujda 60000, Morocco.*

<sup>c</sup>*ICGM, CNRS, Univ Montpellier, ENSCM, Montpellier, France.*

<sup>d</sup>*Laboratory of Biochemistry, Faculty of Sciences, Mohammed First University, 60 000 Oujda, Morocco.*

Corresponding author: Abdelkader Et-touhami

Tel: (+212) 667126373; Fax :(+212) 536500603; E-mail: [touhami\\_52@yahoo.fr](mailto:touhami_52@yahoo.fr)

## Abstract

Two new organotin (IV) bipyrazole-dicarboxylate macrocyclic complexes, **C1** ( $C_{58}H_{100}N_8O_{10}Sn_4$ ) and **C2** ( $C_{58}H_{100}N_8O_{12}Sn_4, 4 H_2O$ ), **are** synthesized by reaction of the bipyrazole-dicarboxylic acids **L1** = 1,1'-(propane-1,3-diyl)bis(5-methyl-1H-pyrazole-3-carboxylic acid) and **L2** = 1,1'-(2-hydroxypropane-1,3-diyl)bis(5-methyl-1H-pyrazole-3-carboxylic acid) with oxide di-(n-butyl)tin. The structure of these complexes **is** characterized using NMR, IR and UV-visible spectroscopies as well as single crystal X-ray diffraction. Compound **C1** crystallizes within the triclinic symmetry in space group  $P\bar{1}$  with  $a = 12.9410(5)$ ,  $b = 13.6143(5)$ ,  $c = 22.7675(8)$  Å,  $\alpha = 92.981(1)$ ,  $\beta = 91.180(1)$ ,  $\gamma = 116.966(1)^\circ$ , while **C2** crystallizes within the rhombohedral symmetry in space group  $R\bar{3}$  with  $a = b = 29.4419(5)$ ,  $c = 23.0326(5)$  Å,  $\alpha = \beta = 90$  and  $\gamma = 120^\circ$ . The analysis by X-ray crystallography diffraction reveals that both complexes are centrosymmetric macrocycles and contain a tetra-nuclear four-fold ladder-like organo-oxotin cluster. Two Sn atoms are found to be five-coordinated while the two others are four-coordinated. The antifungal activity of these metal-cyclic compounds **C1** and **C2** **is** examined and compared to that of the corresponding ligands against the pathogenic strain *Fusarium oxysporum f. sp. albedinis*. The complexes **C1** and **C2** possess an interesting fungicidal power even higher than the ligands **L1** and **L2**.

**Keywords:** Organotin (IV) compound; Synthesis; Bipyrazole-dicarboxylic Acid; Crystal Structure; Antifungal Activity; Macrocyclic.

## 1. Introduction

Organotin (IV) carboxylate complexes have generated a lot of interest among the scientific community over the past 20 years.<sup>1-6</sup> This is due to their structural diversity and their potential application in several fields,<sup>7-9</sup> especially in medicinal chemistry.<sup>8,9</sup> In fact, the literature reports that organotin carboxylates can act as antitumor,<sup>8, 9</sup> antiviral,<sup>10, 11</sup> antifungal,<sup>12, 13</sup> antibacterial,<sup>14, 15</sup> anti-proliferative,<sup>16, 17</sup> anti-inflammatory,<sup>18</sup> and antioxidant potent agents.<sup>19,20</sup>

Among the studies reporting on the various types of organotin complexes, only a few describe the synthesis and characterization of macrocyclic organotin compounds. Chandrasekhar et al. present macrocycle-containing coordination polymers elaborated by condensing the 3,5-pyrazole dicarboxylic acid with di- and tri-organotin substrates.<sup>21</sup> They also communicate on the synthesis of one- and two-dimensional coordination polymers that contain organotin macrocycles by condensation of (n-Bu<sub>3</sub>Sn)<sub>2</sub>O with several pyridine dicarboxylic acids.<sup>22</sup> In 2011, Du and coworkers have reported the synthesis of six new organotin carboxylates based on derivatives of the 1,3-benzenedicarboxylic and 1,4-benzenedicarboxylic acids.<sup>23</sup> One of these compounds is shown to be a more efficient antitumor agent against HeLa than the cis-platinum used clinically. Moreover, Sougoule et al. describe the synthesis and characterization of a novel macrocyclic organotin carboxylate prepared by reaction of di-(n-butyl)tin oxide with the 3-(carboxy-methoxy-phenoxy) acetic acid.<sup>24</sup> Their study has also shown a good antitumor activity for this complex against HeLa cells. The elaboration of an organotin(IV) macrocycle based on (1,3,4-thiadiazole-2,5-diylthio) diacetic acid is also published by Yan et al. who have evaluated its antitumor activity against A549, HeLa and HepG-2 cells.<sup>25</sup> Recently, Rojas-León et al. reported the synthesis and the characterization of a family of tin-based compounds, 21- and 22-membered

macrocycles, which contain 2,5-pyridine dicarboxylate, 3,5-pyridine dicarboxylate and piperazine moieties.<sup>26</sup>

On the other hand, bipyrazolic compounds bearing two carboxylic groups (**Fig. 1**) are of increased interest due to their abilities to form stable complexes with heavy metals, such as copper and cobalt.<sup>27-29</sup>

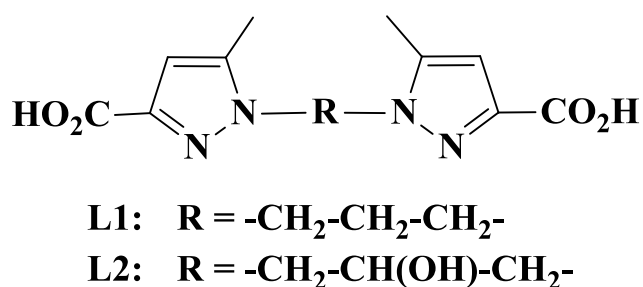


**Fig. 1** Examples of bipyrazolic dicarboxylic acids

However, and to the best of our knowledge, no study reports the synthesis of organotin macrocyclic compounds based on bipyrazole functionalized by dicarboxylic groups.

Thus, this paper presents a pioneering work with the synthesis and characterization of two organotin macrocycles based on such bipyrazolic ligands (**Fig. 1**), which differ by the nature of the spacers between pyrazolic rings. The subsequent modifications in the crystal structures of the two complexes are discussed. The antifungal activity of these complexes is also examined against the pathogenic fungus *Fusarium oxysporum f. sp. albedinis* compared to their corresponding ligands.

## 2. Experimental

### 2.1. General and instrumental

All reagents and solvents were purchased from Sigma-Aldrich and used as received. A spectrometer BRÜKER AC 300 was used to record the NMR spectra. Spin resonances are given in the form of chemical shifts ( $\delta$ ) in parts per million (ppm) with reference to the

residual peak of the solvent used as an internal standard, namely CDCl<sub>3</sub> 7.27 ppm and DMSO-d<sub>6</sub> 2.50 ppm for <sup>1</sup>H NMR, and 77 ppm 39.5 ppm for <sup>13</sup>C NMR. Spin multiplicity is presented by s = singlet, d = doublet, t = triplet, q = quartet, m = multiplet. The melting point (uncorrected) was recorded in a capillary using IA9100 (Electrothermal) apparatus. Elemental analysis was carried out on EA 3000 analyzer. The FTIR spectra were acquired on a Shimadzu FTIR 8400s spectrophotometer and the UV-Vis spectra on a Shimadzu Europe - UV-1650PC equipment.

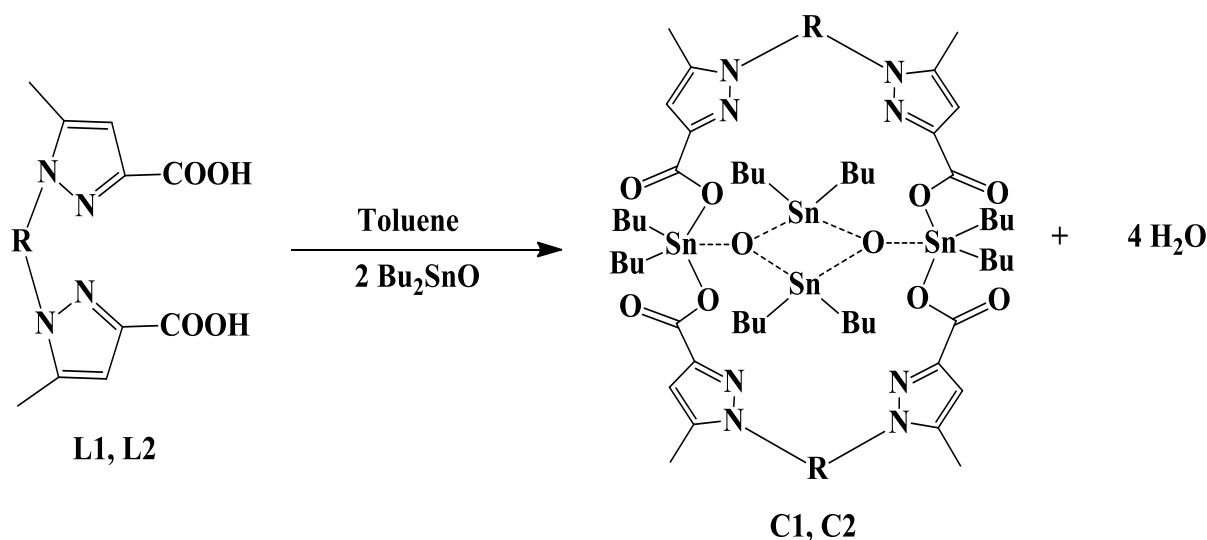
## 2.2. Synthesis

### 2.2.1. Synthesis of ligands **L1** and **L2**

The two ligands 1,1'-(propane-1,3-diyl)bis(5-methyl-1H-pyrazole-3-carboxylic acid) **L1** and 1,1'-(2-hydroxypropane-1,3-diyl)bis(5-methyl-1H-pyrazole-3-carboxylic acid) **L2** were synthesized following the procedure already described in our previous works.<sup>27,29</sup>

### 2.2.2. Synthesis of organotin (IV) carboxylates **C1** and **C2**

The details of the synthetic experiments to complexes **C1** and **C2** are displayed in Scheme 1.



**L1; C1:** R =  $-\text{CH}_2-\text{CH}_2-\text{CH}_2-$   
**L2; C2:** R =  $-\text{CH}_2-\text{CH}(\text{OH})-\text{CH}_2-$

**Scheme 1.** Synthesis pathway of tin complexes **C1-C2**.

#### 2.2.2.1. Synthesis of macrocyclic complex **C1**

A mixture of di-n-butyltin oxide (1 mmol) and **L1** (0.5mmol) was heated under reflux in toluene (50 mL) for 10h in a Dean-Stark apparatus for azeotropic removal of the water formed in the reaction. After cooling to room temperature, the solution was filtered. Suitable colorless crystals were obtained by slow evaporation of the solvent. **Yield** = 67%. **mp** = 104-105 °C. **<sup>1</sup>H NMR** (300MHz, DMSO- $d_6$ )  $\delta$ : 0.62-0.81 (t, 24 H,  $J$  = 8 Hz,  $\text{CH}_3$ ); 1.29–1.60 (m, 48H,  $\text{CH}_2\text{CH}_2\text{CH}_2$ ); 2.25 (s, 12H,  $\text{CH}_3\text{-Pz}$ ); 2.41 (m, 4H,  $-\text{CH}_2-\text{CH}_2-\text{N}$ ); 4.10 (t, 8H,  $J$  = 6 Hz,  $-\text{CH}_2-\text{N}$ ); 6.53 (s, 4H, HPz). **<sup>13</sup>C NMR** (75 MHz, DMSO- $d_6$ )  $\delta$ : 11.27 ( $\text{CH}_3\text{-Pz}$ ); 14.03 ( $\text{CH}_2-\text{CH}_3$ ); 26.06 ( $\text{CH}_2-\text{CH}_2-\text{N}$ ); 26.91, 27.07, 27.47, 28.3, 28.44 ( $\text{CH}_2-\text{CH}_2-\text{CH}_2$ ); 46.43 ( $-\text{CH}_2-\text{N}$ ); 108.42 ( $\text{CH-Pz}$ ); 138.85 ( $\text{CH}_3-\text{C}=\text{C}$ ); 145.30 ( $\text{C}-\text{C}=\text{O}$ ); 166.28 ( $\text{C}=\text{O}$ ). **IR** ( $\text{cm}^{-1}$ ): 1630  $\nu_{\text{as}}(\text{COO})$ ; 1420  $\nu_{\text{s}}(\text{COO})$ ; 560  $\nu(\text{Sn}-\text{C})$ ; 465  $\nu(\text{Sn}-\text{O})$ . **Anal.** Calcd for  $\text{C}_{58}\text{H}_{100}\text{N}_8\text{O}_{10}\text{Sn}_4$ : C, 45.11; H, 6.53; N, 7.26; O, 10.36; Found: C, 45.14; H, 6.56; N, 7.29; O, 10.38.

### 2.2.2.2. Synthesis of macrocyclic complex **C2**

The complex **C2** was synthesized in a similar way to **C1**. Suitable colorless crystals were obtained by slow evaporation of the solvent. Yield = 62%. mp = 97-98 °C. <sup>1</sup>H NMR (250 MHz, DMSO-*d*<sub>6</sub>) δ: 0.6–1.60 (m, 72H, CH<sub>2</sub>CH<sub>2</sub>CH<sub>2</sub>CH<sub>3</sub>); 1.75 (s, 8H, H<sub>2</sub>O); 2.27 (s, 12 H, CH<sub>3</sub>Pz); 3.95-4.24 (m, 8H, CH<sub>2</sub>-CH(OH)-CH<sub>2</sub>); 4.73 (m, 2H, HO-CH-CH<sub>2</sub>-Pz); 5.57 (d, 2H, *J*= 6Hz, HO-CH-CH<sub>2</sub>); 6.45 (s, 4H, HPz). <sup>13</sup>C NMR (75 MHz, DMSO-*d*<sub>6</sub>) δ: 11.37 (CH<sub>3</sub>Pz); 13.62, 13.64 (CH<sub>2</sub>-CH<sub>3</sub>); 25.85, 26.74, 26.95, 27.45 (CH<sub>2</sub>-CH<sub>2</sub>-CH<sub>2</sub>); 52.45 (CH<sub>2</sub>-CH(OH)-CH<sub>2</sub>); 56.48 (CH<sub>2</sub>-CH(OH)-CH<sub>2</sub>); 108.42 (CH-Pz); 141.63 (CH<sub>3</sub>-C=C); 144.55 (C-C=O); 165.92 (C=O). IR (cm<sup>-1</sup>): 1630 *v*<sub>as</sub>(COO); 1420 *v*<sub>s</sub>(COO); 560 *v*(Sn-C); 465 *v*(Sn-O). Anal. Calcd for C<sub>58</sub>H<sub>100</sub>N<sub>8</sub>O<sub>12</sub>Sn<sub>4</sub>·4 H<sub>2</sub>O: C, 42.26; H, 6.60; N, 6.80; O, 15.53; Found: C, 42.29; H, 6.64; N, 6.83; O, 15.56.

### 2.3. X-ray crystallography

Crystals suitable for X-ray data collection were selected using a stereo microscope with a polarizing filter. The diffracted intensities were recorded on a 4-circle diffractometer (Bruker D8 Venture) equipped with a Mo K $\alpha$  micro-source (Incoatec I $\mu$ S 3.0, 110 $\mu$ m beam,  $\lambda$  = 0.71073 Å) and a Photon II CPAD detector. Data were handled with the Apex software suite for reduction, absorption corrections (multi-scan SADABS),<sup>30</sup> and the structures were solved and refined using the SHELX programs.<sup>31, 32</sup> For the non-H atoms, all positional and anisotropic displacement parameters were refined while the H-atoms were treated using a riding model with displacement parameters equal to 1.2 (1.5 for -CH<sub>3</sub>) times the *U*<sub>eq</sub> of the parent atom. The crystal data and the main refinement parameters are given in Table 1. The full crystallographic data (CIF files) can be obtained free of charge from the Cambridge Crystallographic Data Center mentioning the corresponding CCDC numbers.<sup>33</sup>

**Table 1.** Crystal data and refinement parameters.

Compound	C <sub>58</sub> H <sub>100</sub> N <sub>8</sub> O <sub>10</sub> Sn <sub>4</sub> (C1)	C <sub>58</sub> H <sub>100</sub> N <sub>8</sub> O <sub>12</sub> Sn <sub>4</sub> , 4 H <sub>2</sub> O (C2)
<i>CCDC number</i>	<b>2070454</b>	<b>2070462</b>
<i>System, space group</i>	<b>Triclinic, P<math>\bar{1}</math></b>	<b>Rhombohedral, R3</b>
<i>Unit cell dimensions Å, °</i>	<b>a = 12.9410(5), b = 13.6143(5), c = 22.7675(8), <math>\alpha</math> = 92.981(1), <math>\beta</math> = 91.180(1), <math>\gamma</math> = 116.966(1)</b>	<b>a = b = 29.4419(5), c = 23.0326(5), <math>\alpha</math> = <math>\beta</math> = 90, <math>\gamma</math> = 120</b>
<i>Volume Å<sup>3</sup></i>	<b>3565.9(2)</b>	<b>17290.4(7)</b>
<i>Temperature K</i>	<b>296(2)</b>	<b>173(2)</b>
<i>M, Z</i>	<b>1543.21, 2</b>	<b>1648.28, 9</b>
<i>Calculated density Mg/m<sup>3</sup></i>	<b>1.437</b>	<b>1.422</b>
<i>Abs. coefficient mm<sup>-1</sup></i>	<b>1.439</b>	<b>1.346</b>
$\theta$ range °	2.455 to 27.502	1.940 to 27.993
Index ranges	-16 ≤ h ≤ 16, -17 ≤ k ≤ 17, -29 ≤ l ≤ 29	-38 ≤ h ≤ 38, -38 ≤ k ≤ 33, -30 ≤ l ≤ 30
Unique reflections.	16311 [R <sub>int</sub> = 0.0418]	18571 [R <sub>int</sub> = 0.0418]
Data / restraints / params.	16311 / 54 / 736	18571 / 19 / 817
Goodness-of-fit on F <sup>2</sup>	1.045	1.096
Flack parameter	-	0.44(3)
Final R indices [I > 2σ(I)]	R1 = 0.0426, wR2 = 0.1191	R1 = 0.0310, wR2 = 0.0780
R indices (all data)	R1 = 0.0654, wR2 = 0.1396	R1 = 0.0450, wR2 = 0.0890
Extinction coefficient	0.0070(7)	0.0089(9)
Residual density e.Å <sup>-3</sup>	4.086 and -0.749	1.352 and -0.810

The colorless and diamond-shaped crystals of **C1**, obtained by recrystallization from a mixture of solvents (ethanol/diethyl-ether), were cut into small parts and two fragments were used for data collection at room temperature. Subsequent low-temperature recording failed, giving only a data overlay of multiple components, even for crystals grown from ethanol/dichloromethane solvents. It appears that lowering the temperature causes a misalignment of components generated by cleavage during the crystal cutting operation. Despite this drawback, the structure could be solved in the P $\bar{1}$  centrosymmetric space group (according to statistics) from the data collected at ambient temperature. The refinement of the main part of the molecule converged to R1 ~ 10%, then the C atoms of the butyl groups attached to tin atoms were found in the Fourier difference. Most aliphatic branches refine normally, except three which have stability issues that could not be resolved in the non-centrosymmetric space group P1. Then geometrical DFIX restraints were applied to the C—C

bonds of all the butyl groups. The presence of large ellipsoids would require consideration of disorder to further improve the refinement, but this was not possible with the current data sets.

The data collection was performed both at room temperature and 173K for fragments of the colorless crystals of **C2**. Statistics indicate centrosymmetry and data appear to be rhombohedral with a surprisingly high symmetry compared to **C1**. **The unit cell was defined with the hexagonal axes ( $a = b = 29.44$ ,  $c = 23.03$  Å,  $\alpha = \beta = 90$ ,  $\gamma = 120$ ) as conventionally done for rhombohedral systems, preferred to the rhombohedral axes of the reduced cell ( $a = b = c = 18.7$  Å,  $\alpha = \beta = \gamma = 104^\circ$ ).** The structure was initially solved in the centrosymmetric space group  $R\bar{3}$  but some abnormal/strange behavior was noted at the butyl chain atoms in the refinements even when using the low-temperature data set. **Attempts to model and to solve such intricate disorder remained unsuccessful.** This situation resembles that of an example of twinning reported by Sheldrick<sup>34</sup> but, although a (pseudo)merohedral twin can be suspected, no twin law could be found and none of the attempts considering alternative lattices and/or space groups was fully satisfactory. **In fact, the 3-fold symmetry could be generated by several crystal components having potentially lower symmetry, as is the case for the monoclinic crystals in this example<sup>34</sup> appearing to be rhombohedral from the diffraction symmetry. Hence, the structure which is given here in the non-centrosymmetric space group  $R3$  may not be described with its "true" symmetry/cell. Structural validation is to be provided with the study of better crystallized and higher quality crystals in future works.** Four water molecules can be located around the cell origin from the Fourier difference, their H-atoms are involved in H-bonds and refined using DFIX instructions. Likewise in the nearby butyl chains, restraints were applied to the C–C distances involving atoms with fairly large ellipsoids. **In addition to this phenomenon related to the great mobility of the alkyl chains, small residual density peaks distributed along the  $c$ -axis indicate that the accessible void remaining around the**

**origin (3a positions) could be filled with additional water molecules. Such molecules would be in more disordered positions due to their lack of involvement in H-bonds.** Or else, the molecular arrangement induced by the solvent molecules present in these channels could remain strongly stabilized by the hydrogen bonds even after total or partial elimination of the solvent (disordered residual solvent molecules).

#### **2.4. Antifungal activity**

The *in vitro* antifungal activity of the di-n-butyltin (IV) dicarboxylate complexes (**C1**, **C2**) and their corresponding ligands (**L1**, **L2**) **was** examined against fungus *Fusarium oxysporum f. sp. albedinis* (FAO) using the agar diffusion technique, as reported in our recent work.<sup>13</sup> Potato dextrose agar (PDA) medium was mixed with different volumes (40, 160, and 500  $\mu$ L) of DMSO solutions of the complexes and the corresponding ligands. Then, discs (6 mm in diameter) of the microorganism (FAO) were put in the middle of these Petri plates. After incubation at 28 °C for 7 days, inhibition percentages (% I) of the growth rate were calculated as follows:  $\% I = ((D_o - D_x) / D_o) \times 100$ , where  $D_o$  and  $D_x$  are the respective diameters (cm) of the FOA in the absence and presence of the product tested. Benomyl was used as the positive control.

### **3. Discussion**

#### **3.1. NMR spectroscopy**

In the <sup>1</sup>H NMR spectra of the macrocyclic organotin carboxylates **C1** and **C2**, we note the absence of signal associated with the carboxyl proton that appears around 12.5 ppm for the ligands **L1** and **L2**.<sup>27,29</sup> This evidences the participation of both carboxylic groups in the coordination of the tin atom in these complexes. On the other hand, the rest of the protons belonging to the ligands keep the same integration and multiplicities as in the free ligands. The protons of the butyl groups attached to the Sn atom are found at chemical shifts from 0.6

to 1.8 ppm, in a range where some signals are duplicated twice (**Fig. 2**). Furthermore, the NMR spectrum of the complex **C2** displays a massive pic at 1.65 ppm, a signal which is attributed to the protons of the four water molecules resulting from the reaction.

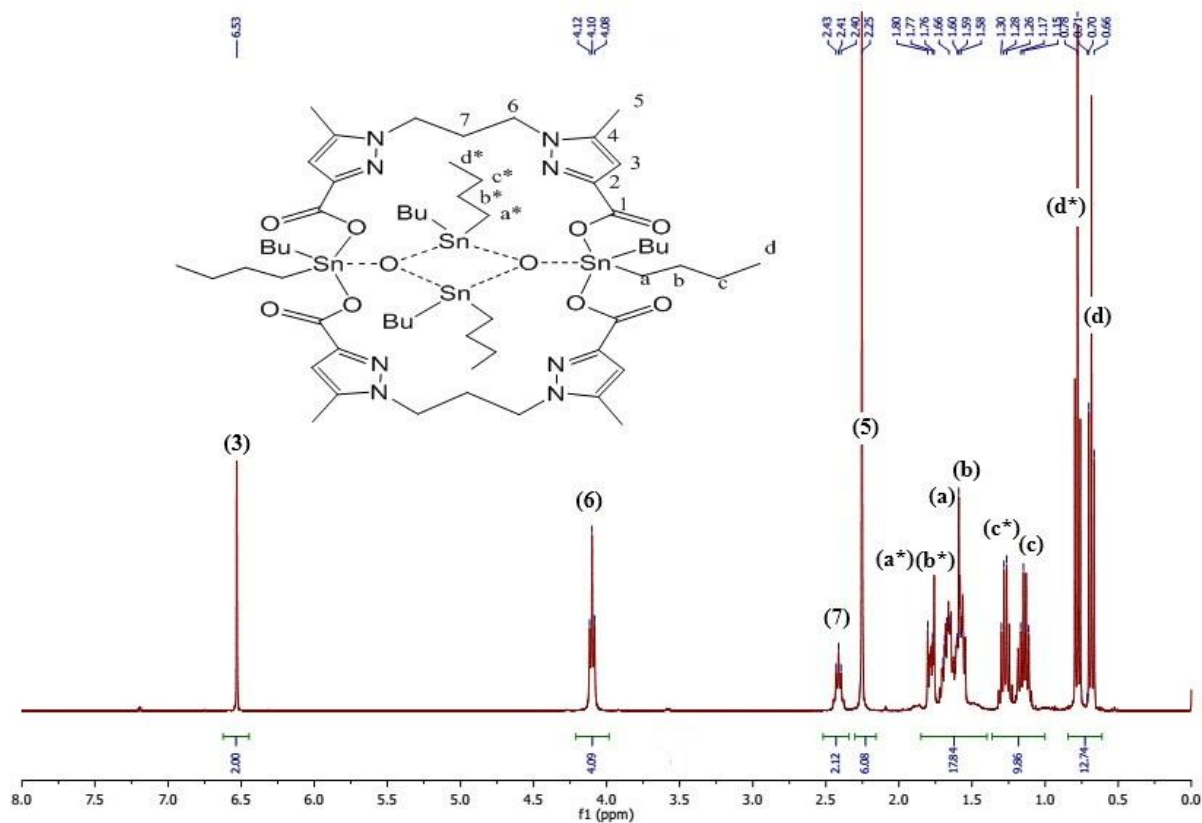


**Fig. 2.** <sup>1</sup>H NMR spectrum of **C1**.

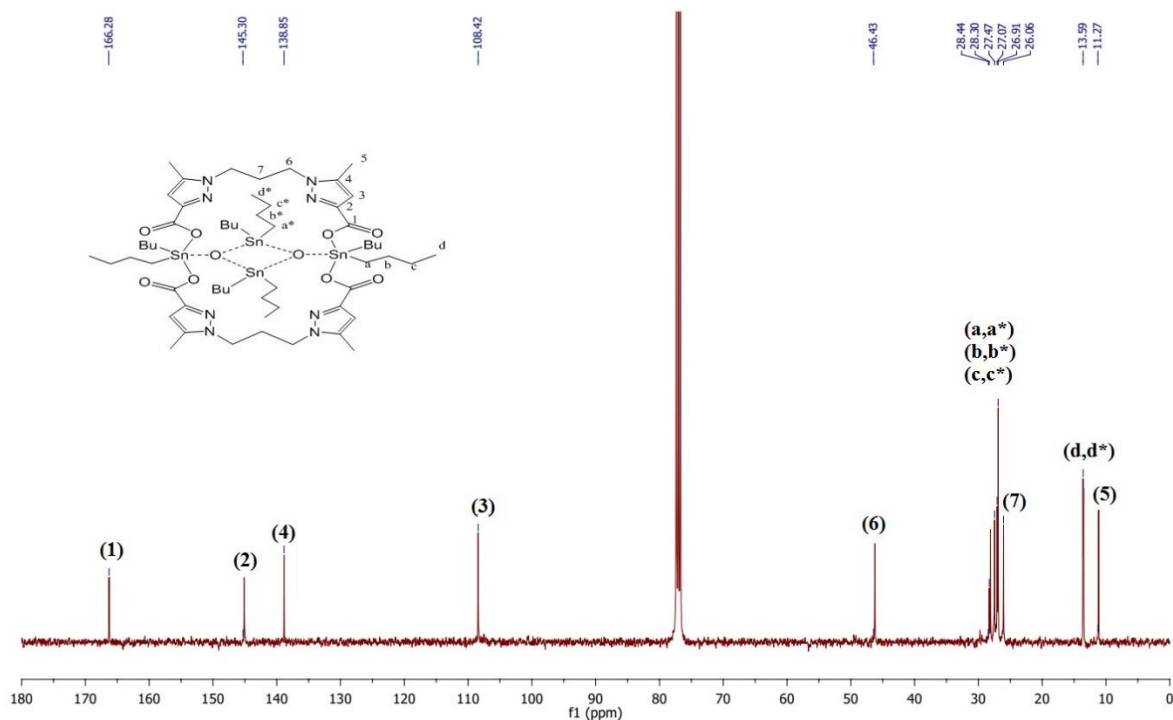


**Fig. 3.**  $^{13}\text{C}$  NMR spectrum of **C1**.

This proves the presence of two butyl categories and the result agrees with the crystal structures determined for the complexes **C1** and **C2**. As well, the above remark is also confirmed by the  $^{13}\text{C}$  NMR spectra (**Fig. 3.**) of both complexes in which is observed the duplication of some carbon atom signals of the butyl group. Also, the signals corresponding to the carboxyl carbon atoms of the complexes **C1** and **C2**, appearing at 166 and 167 ppm respectively, show a slight downfield shift compared to their free ligands **L1** and **L2**. These results are very consistent with those reported in several related works and such behavior is due to a transfer of the electron density from the ligands towards the tin atoms.<sup>35</sup>

### 3.2. FTIR and UV-visible spectroscopy

In the FTIR spectra of the complexes **C1** (**Fig. 4**) and **C2**, no large band in the range of  $3500\text{--}2850\text{ cm}^{-1}$  is observed attributed to O-H stretching vibrations as in free ligands. This indicates that the Sn-to-ligand bond is established *via* these sites.

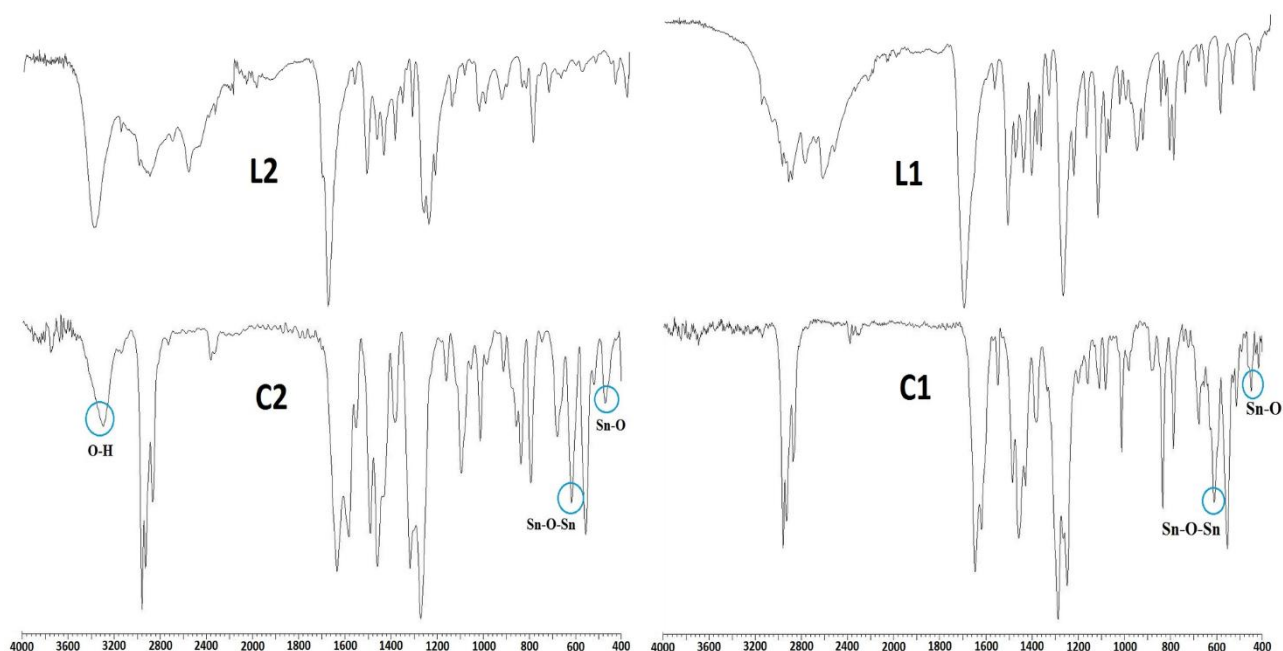


**Fig. 4.** FTIR spectra of **L1** ligand and their corresponding complexes **C1**.

In addition, strong absorption peaks are observed at  $\sim 1670$  and  $1463\text{ cm}^{-1}$ , they are attributed to the asymmetric and symmetric vibrations of the COO fragments (**Fig. 3**). The difference between the asymmetric and symmetric COO stretching vibrations,  $\Delta\nu = \nu_{\text{as}}(\text{OCO}) - \nu_{\text{s}}(\text{OCO})$  is known as a good tool to determine the mode of coordination of the ligands carboxylate with metals.<sup>23</sup> The  $\Delta\nu$  values higher than  $200\text{ cm}^{-1}$  are typical for monodentate complexes. In the present case, the values of  $210$  and  $215\text{ cm}^{-1}$  for **C1** and **C2**, respectively, prove the monodentate coordination mode for both the carboxylic ligands **L1** and **L2**.<sup>13</sup> On the other hand, the FTIR spectra of the two complexes **C1** and **C2** present bands at  $640$  and  $631\text{ cm}^{-1}$ . These bands are attributed to  $\nu(\text{Sn-O-Sn})$  stretching vibrations, which evidences the presence of diorganotin dicarboxylates containing  $\text{Sn}_2\text{O}_2$  units.<sup>13, 35</sup> The conclusions drawn from the FTIR spectroscopy analysis are also in agreement with the structures obtained from X-ray crystallography.

The electronic absorption spectra have also been recorded for the two complexes in methylene chloride using UV-visible spectroscopy. The acquired spectra (**Fig. 5**) are found

almost similar and show absorption peaks in the region 235-280 nm resulting from the  $\pi$ - $\pi^*$  and the  $n \rightarrow \pi^*$  transitions.<sup>36</sup>

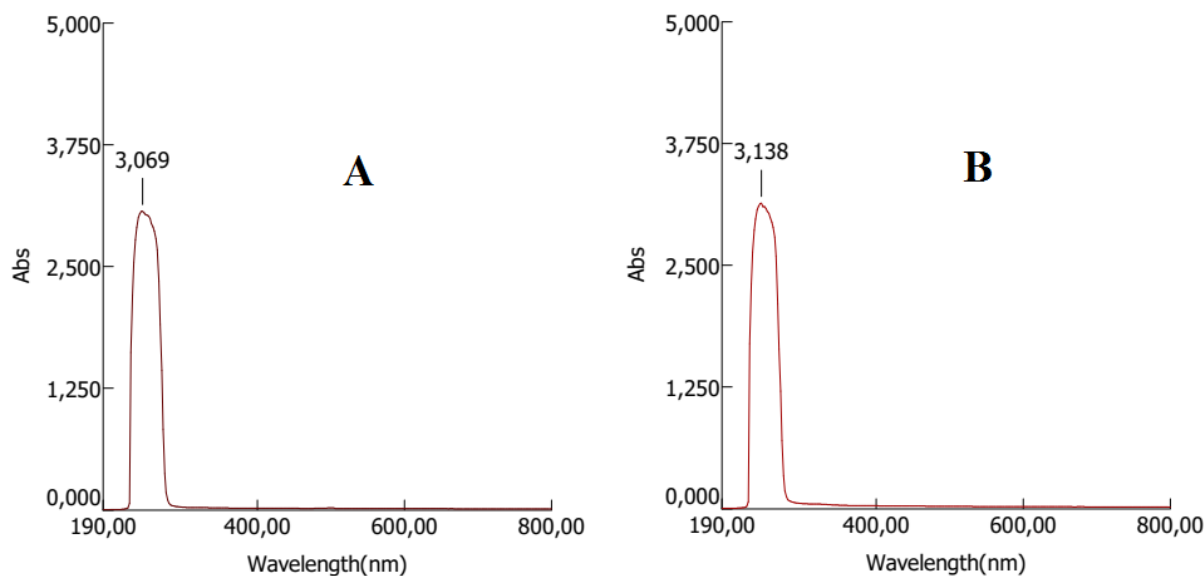


**Fig. 5.** UV-visible spectra of **C1** (A) and **C2** (B).

### 3.3. Crystal structures of **C1** and **C2**

The triclinic  $P\bar{1}$  unit cell of **C1** contains two independent molecules  $\text{Sn}_4\text{N}_8\text{O}_{10}\text{C}_{58}\text{H}_{100}$  otherwise formulated  $\text{Sn}_4\text{N}_8\text{O}_{10}\text{C}_{26}\text{H}_{28}\text{R}_8$  ( $\text{R} = \text{C}_4\text{H}_9$ ) since each Sn atom bears two butyl groups. Only one independent molecule of the formula  $\text{Sn}_4\text{N}_8\text{O}_{12}\text{C}_{58}\text{H}_{100}$  (or  $\text{Sn}_4\text{N}_8\text{O}_{12}\text{C}_{26}\text{H}_{28}\text{R}_8$ ) is found in the noncentrosymmetric R3 rhombohedral cell of **C2**. As shown in the ORTEP<sup>37</sup> drawing given in **Fig. 6**, the butyl chains are placed above and below the midplane of the molecules, both represented with their nearly planar  $\text{Sn}_4\text{O}_6$  central cores approximately in the horizontal plane. The **C2** molecule differs from the **C1** molecule by the  $-\text{OH}$  group attached to the chain connecting the two pyrazole rings. Moreover, it crystallizes with water molecules to which it interacts through hydrogen bonds, as shown in **Fig. 6**. This could be the reason behind such a difference in the crystal symmetry between the two structures.

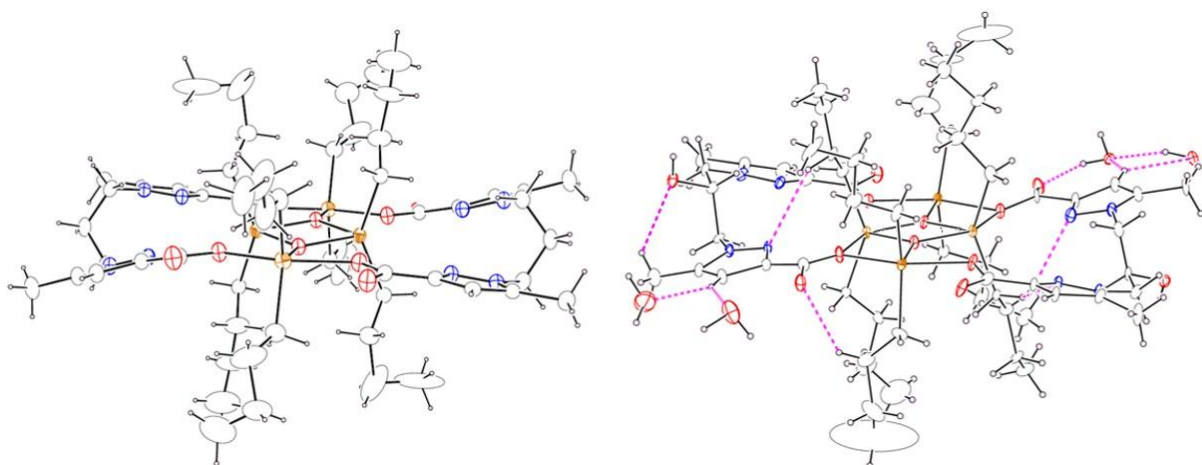


**Fig. 6.** The molecules  $\text{Sn}_4\text{N}_8\text{O}_{10}\text{C}_{26}\text{H}_{28}\text{R}_8$  (**C1**, left) and  $\text{Sn}_4\text{N}_8\text{O}_{12}\text{C}_{26}\text{H}_{28}\text{R}_8$  (**C2**, right) ( $\text{R} = \text{C}_4\text{H}_9$ ). The H-bonds involving a **C2** molecule and four water molecules are drawn as dashed lines and the ellipsoids are represented at 15% probability.

In the triclinic unit cell of **C1**, the two independent molecules are placed at the special positions  $1a$  (0 0 0) and  $1h$  ( $\frac{1}{2}$   $\frac{1}{2}$   $\frac{1}{2}$ ) on inversion centers and therefore are centrosymmetric. Instead, the molecule of **C2** does not display an inversion center. Looking at the molecular representations given in **Fig. 7**, one first notices two types of Sn atoms, either coordinated with 2 or 3 oxygen neighbors. The existence of two coordination modes for the tin atoms was later confirmed by spectroscopic and RMN studies. Also, the molecules differ in geometry, especially at their  $\text{Sn}_4\text{O}_6$  central cores. The first molecule of **C1** displays a fairly regular oxygen arrangement around the Sn11 and Sn12 centers while the environment is much more distorted around the Sn21 and Sn22 centers within the second molecule of **C1**. The rest of the molecule therefore also differs. Such variations arise from molecular packing effects in the crystal and intermolecular interactions in the solid-state.

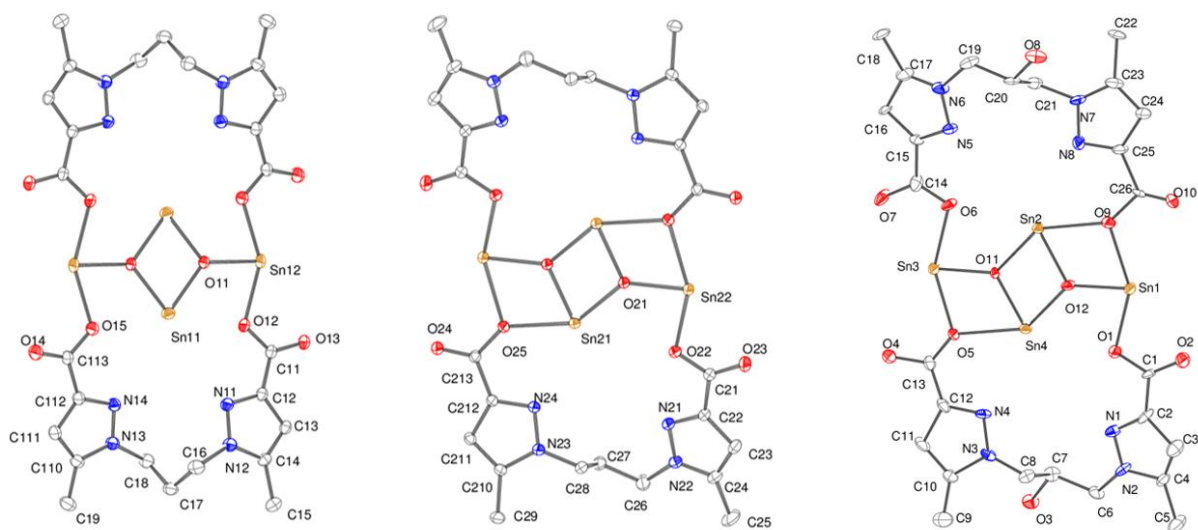


**Fig. 7.** The centrosymmetric **C1** molecules (left and middle) and the non-centrosymmetric **C2** molecule (right). (Atoms are labeled and butyl chains attached to Sn are omitted for clarity).

According to the Pearson database, the experimental Sn-O bonds are reported in the typical range of 1.90-2.25 Å. This means that the Sn11 atom is bi-coordinated and the Sn12 atom is tri-coordinated in the first molecule of **C1** (**Fig. 8**), while each of the Sn atoms of the second molecule (Sn21 and Sn22) is involved in two classical bonds and one long interaction of about 2.3 Å, out of range given for bond distances. The longer Sn—O interatomic distances of ~2.6 and ~3.3 Å cannot be considered as bonds. The experimental geometry of the **C2** molecule can be described with three classical Sn—O bonds around Sn1 and Sn3 atoms and two classical bonds plus a long and most certainly non-bonding Sn—O interaction of ~2.4 Å for the Sn2 and Sn4 atoms. It would be useful to compare these molecular geometries with that of an isolated molecule to assess the stresses to which molecules are subjected in the crystalline solid state. This is why we performed a geometry optimization for the **C1** molecule in a DFT calculation (Dmol<sup>3</sup>, LDA/PWC functional, DND basis set). The distances within the Sn<sub>4</sub>O<sub>6</sub> central core are given in **Fig. 8** for the optimized molecule comparatively with the

experimental distances measured for the molecules in the **C1** and **C2** crystal structures. In the optimized isolated molecule, Sn1 atom is involved in two Sn—O bonds of 2.068 and 2.077 Å and Sn2 atom in three Sn—O bonds from 2.002 to 2.216 Å, all in the range of classical bonds, and the oxygen atoms distant by more than 2.6 Å do not form bonds. Such a comparison provides information on how the molecule deforms in the crystal causing these oxygen atoms to move closer or further away from the Sn centers.

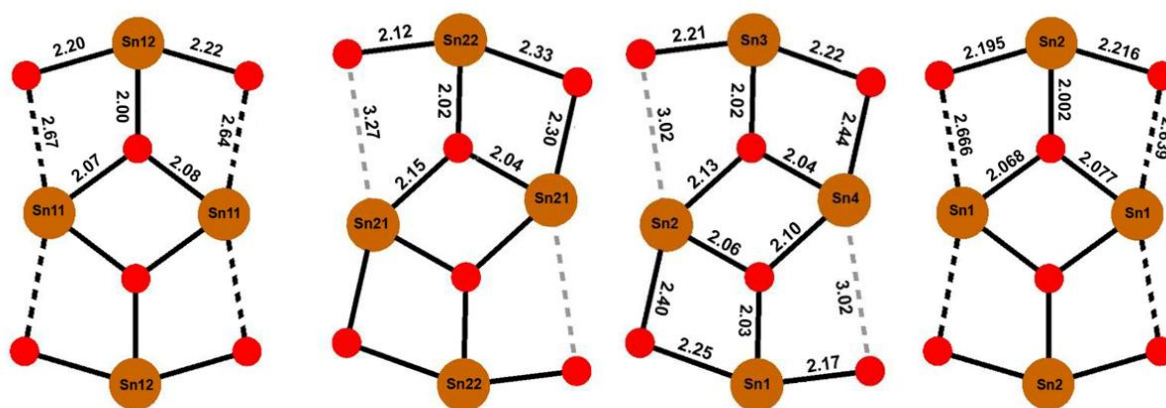


**Fig. 8.** The Sn—O distances within the Sn<sub>4</sub>O<sub>6</sub> central core in (*left to right*) the two molecules of **C1**, the molecule of **C2**, and the optimized isolated molecule of **C1**.

### 3.4. Antifungal activity

The organotin compounds **C1-C2** and their corresponding ligands **L1-L2** have been examined *in vitro* for their antifungal activity against *Fusarium oxysporum f. sp. Albedinis* (FOA) fungal. First, as can be seen in the results obtained collated in **Table 2**, the dose used affects the antifungal activity of the complexes and ligands.

**Table 2.** Antifungal activity of **C1** and **C2** complexes and corresponding **L1** and **L2** ligands.

Compound	Volume withdrawn ( $\mu\text{l}$ )	Strain diameter (cm)	Inhibition %
<b>C1</b>	40	8,5	<b>0,00</b>
	160	8,5	<b>0,00</b>
	500	0,8	<b>90,59</b>
<b>C2</b>	40	8,5	<b>0,00</b>
	160	8,5	<b>0,00</b>
	500	2,3	<b>72,94</b>
<b>L1</b>	40	8,5	<b>0,00</b>
	160	8,5	<b>0,00</b>
	500	1,4	<b>83,53</b>
<b>L2</b>	40	8,5	<b>0,00</b>
	160	8,5	<b>0,00</b>
	500	6,5	<b>23,53</b>
<b>Benomyl</b>	40	2,3	<b>54,00</b>
	160	1,1	<b>78,00</b>
	500	0,3	<b>94,00</b>

The bipyrazole dicarboxylic acid ligands **L1-L2** possess no activity towards FOA for volume withdrawal of 40 and 160  $\mu\text{l}$ . An increase in volume up to 500  $\mu\text{l}$  confers **L1** some antifungal potency, while it remains rather weak for **L2**. The present finding proves the effect of the nature of the spacer between the two pyrazolic rings on the antifungal activity as is reported in one of our recent studies.<sup>13</sup> For the complexes **C1** and **C2**, it is clear that the coordination of di-n-butyltin by ligands **L1** and **L2** does not affect the antifungal activity at the volume withdrawal of 40 and 160  $\mu\text{l}$  which remains zero. By contrast, both complexes have shown activity at 500  $\mu\text{l}$  with values that are different. This indicates that the nature of the spacer between the two pyrazolic rings still affects the antifungal activity, as well as the presence of di-n-butyltin. The literature reports that the antifungal activity of tin complexes increases with the increase of their lipid-solubility.<sup>38, 39</sup> This give them the possibility to penetrate through the cytoplasmic membrane and then to become a possible site of action.<sup>40, 41</sup> Thus, the low activity of **C2** can be explained by a lower lipid-solubility compared to that of **C1**. This is due to the presence of a hydroxyl moiety on the spacer between the two pyrazole

cycles. Finally, despite their significant antifungal activities, these complexes remain with lower efficiencies than the positive control, the Benomyl.

#### 4. Conclusion

In this paper, we have presented the synthesis of two new macrocyclic organotin (IV) carboxylates **C1** and **C2** based on bipyrazole dicarboxylic acid, which differ by the nature of spacers between the two pyrazole rings. This difference affects considerably their conformation as revealed by their single crystal X-ray structures. The NMR and FTIR spectroscopies as well as the elemental analyses are perfectly consistent with the structural determinations. The antifungal activity was investigated for the complexes **C1** and **C2** and the corresponding ligands **L1** and **L2** against *Fusariumoxysporum f. sp. albedinis* (FOA) and it depends on the presence of tin, on the nature of the spacer between the two pyrazole rings and on the dose used.

#### Conflicts of interest

No conflict of interest was reported by the authors.

#### Appendix A. Supplementary data

CIF files <CCDC 2070454> for  $C_{58}H_{100}N_8O_{10}Sn_4$  (**C1**) and <CCDC 2070462> for  $C_{58}H_{100}N_8O_{12}Sn_4 \cdot 4 H_2O$  (**C2**) are deposited at Cambridge Crystallographic Data Center.

#### References

1. A. J. Crowe, P. J. Smith and G. Atassi, *Chem. Biol. Interact.*, 1980, **32(1-2)**, 171-178.
2. D. de Vos, R. Willem, M. Gielen, K. E. van Wingerden and K. Nooter, *Metal-Based Drugs*, 1998, **5**, 179–188.
3. M. Nath, S. Pokharia, G. Eng, X. Song and A. Kumar, *J. Organomet. Chem.*, 2003, **669**, 109–123.

4. M. Nath, S. Pokharia, X. Song, G. Eng, M. Gielen, M. Kemmer and D. de Vos, *Appl. Organomet. Chem.*, 2003, **17**, 305–314.
5. A. G. Hadi, K. Jawad, D. S. Ahmed and E. Yousif, *Syst. Rev. Pharm.*, 2019, **10(1)**, 26-31.
6. H. Iqbal, S. Ali and S. Shahzadi, *Cogent Chem.*, 2015, **1(1)**, 1029039.
7. E. R. Tiekink, *Appl. Organomet. Chem.*, 1991, **5(1)**, 1-23.
8. M. Gielen, *Coord. Chem. Rev.*, 1996, **151**, 41-51.
9. M. S. Ahmad, M. Hussain, M. Hanif, S. Ali and B. Mirza, *Molecules*, 2007, **12(10)**, 2348-2363.
10. C. E. Carraher Jr and M. R. Roner, *J. Organomet. Chem.*, 2014, **751**, 67-82.
11. C. E. Carraher, T. S. Sabir, M. R. Roner, K. Shahi, R. E. Bleicher, J. L. Roehr and K. D. Bassett, *J. Inorg. Organomet. Polym. Mater.*, 2006, **16(3)**, 249-257.
12. A. F. Butt, M. N. Ahmed, M. H. Bhatti, M. A. Choudhary, K. Ayub, M. N. Tahir and T. Mahmood, *J. Mol. Struct.*, 2019, **1191**, 291-300.
13. M. Dahmani, A. Et-Touhami, A. Yahyi, T. Harit, D. Eddike, M. Tillard and R. Benabbes, *J. Mol. Struct.*, 2021, **1225**, 129-137.
14. L. Hu, H. Wang, T. Xia, B. Fang, Y. Shen, Q. Zhang, X. Tian, H. Zhou, J. Wu and Y. Tian, *Inorg. Chem.*, 2018, **57(11)**, 6340-6348.
15. T. Sedaghat, M. Yousefi, G. Bruno, H. A. Rudbari, H. Motamedi and V. Nobakht, *Polyhedron*, 2014, **79**, 88-96.
16. M. Nath, R. Yadav, M. Gielen, H. Dalil, D. de Vos and G. Eng, *Appl. Organomet. Chem.*, 1997, **11(9)**, 727-736.
17. D. Kovala-Demertzi, V. Dokorou, A. Primikiri, R. Vargas, C. Silvestru, U. Russo and M. A. Demertzis, *J. Inorg. Biochem.*, 2009, **103(5)**, 738-744.
18. M. Nath, M. Vats and P. Roy, *Inorg. Chim. Acta.*, 2014, **423**, 70-82.

19. A. Corona-Bustamante, J. M. Viveros-Paredes, A. Flores-Parra, A. L. Peraza-Campos, F. J. Martínez-Martínez, M. T. Sumaya-Martínez and Á. Ramos-Organillo, *Molecules*, 2010, **15(8)**, 5445-5459.
20. I. Ahmad, A. Waseem, M. Tariq, C. MacBeth, J. Bacsá, D. Venkataraman and S. Tabassum, *Inorg. Chim. Acta.*, 2020, **505**, 119433.
21. V. Chandrasekhar and R. Thirumoorthis, *Organometallics*, 2009, **28(7)**, 2096-2106.
22. V. Chandrasekhar, C. Mohapatra and R. J. Butcher, *Cryst. Growth Des.*, 2012, **12(6)**, 3285-3295.
23. D. Du, Z. Jiang, C. Liu, A. M. Sakho, D. Zhu and L. Xu, *J. Organomet. Chem.*, 2011, **696(13)**, 2549-2558.
24. A. S. Sougoule, Z. Mei, X. Xiao, C. A. Balde, S. Samoura, A. Dolo and D. Zhu, *J. Organomet. Chem.*, 2014, **758**, 19-24.
25. F. F. Yan, C. L. Ma, Q. L. Li, S. L. Zhang, J. Ru, S. Cheng and R. F. Zhang, *New J. Chem.*, 2018, **42(14)**, 11601-11609.
26. I. Rojas-León, H. Alnasr, K. Jurkschat, M. G. Vasquez-Ríos, G. Gómez-Jaimes, H. Höpfl and R. Santillan, *Organometallics*, 2019, **38(12)**, 2443-2460.
27. S. Radi, A. Yahyi, A. Ettouhami, A. C. Jha, N. N. Adarsh, K. Robeyns and Y. Garcia, *Polyhedron*, 2015, **85**, 383-388.
28. S. Radi, M. El-Massaoudi, H. Benaissa, N. N. Adarsh, M. Ferbinteanu, E. Devlin and Y. Garcia, *New J. Chem.*, 2017, **41(16)**, 8232-8241.
29. T. Harit, H. Abouloifa, M. Tillard, D. Eddike, A. Asehraou and F. Malek, *J. Mol. Struct.*, 2018, **1163**, 300-307.
30. Bruker, APEX3. Version 2017.3-0, Bruker AXS, Inc., Madison, Wisconsin, USA, 2017.
- 31. G. M. Sheldrick, *Acta Crystallogr.*, 2015, **A71**, .3-8.**
- 32. G. M. Sheldrick, *Acta Crystallogr.*, 2015, **C71**, 3-8.**

33. <http://www.ccdc.cam.ac.uk/conts/retrieving.html> (or from the CCDC, 12 Union Road, Cambridge CB2 1EZ, UK; Fax: +44 1223 336033; E-mail: deposit@ccdc.cam.ac.uk)
34. R. Herbst-Irmer and G. M. Sheldrick, *Acta Crystallographica Section B: Structural Science*, 1998, **54(4)**, 443-449.
35. X. Du, R. Zhang, Q. Li, S. Cheng, Y. Li, J. Ru and C. Ma, *J. Organomet. Chem.*, 2020, 121654.
36. T. Harit, M. Dahmani, S. Gaamouche, F. Malek, M. Dusek, A. Manseri and A. Asehraou, *J. Mol. Struc.*, 2019, 1176, 110–116.
37. L.J. Farrugia, ORTEP-3 for Windows, an update, *J. Appl. Crystallogr.*, 2012, **45**, 849-854.
38. D. C. Menezes, F. T. Vieira, G. M. De Lima, J. L. Wardell, M. E. Cortés, M. P. Ferreira and A. Vilas Boas, *Appl. Organomet. Chem.*, 2008, **22(4)**, 221-226.
39. E. N. Iornumbe, S. G. Yiase, J. Audu and B. O. Ozide, *Journal of Chemical Society of Nigeria*, 2018, 43(4).
40. J. S. White and J. M. Tobin, *Environ. Sci. Technol.*, 2004, **38**, 3877-3884.
41. J. S. White and J. M. Tobin, *J. Appl. Microbiol. Biotechnol.*, 2004, **63**, 445-451.